ChemComm

COMMUNICATION

View Article Online
View Journal | View Issue

Cite this: *Chem. Commun.*, 2019, 55, 3387

Received 3rd January 2019,
Accepted 19th February 2019

DOI: 10.1039/c9cc00046a

rsc.li/chemcomm

An ethyl methyl sulfone co-solvent eliminates macroscopic morphological instabilities of lithium metal anode†

Woochul Shin,[a] Kang Pyo So,[b] William F. Stickle,[c] Cong Su,[b] Jun Lu,[d] Ju Li*[b] and Xiulei Ji*[a]

Lithium metal anodes suffer from a short cycle life, and the parasitic reactions of lithium with electrolytes are widely observed. Common sense is to avoid such reactions. Herein, we head in the opposite direction by using an oxidizing co-solvent, ethyl methyl sulfone, in the electrolyte, which addresses the 'dendrite' issue entirely, resulting in a dense and macroscopically smooth surface morphology of the plated lithium. However, a dendrite-free lithium metal anode does not necessarily exhibit a high coulombic efficiency.

Lithium metal anode (LMA) materials are considered to be the ultimate solution to facilitate the long-driving range of electric vehicles (EV). The challenges of LMA are twofold: (1) lithium morphological instabilities (LMI) during plating/stripping that may cause shorting and thermal runaway and (2) the low coulombic efficiency (CE). LMI can be categorized into 'dendrite or tip grown' (mode III), stress-derived 'whisker or root grown' (mode II), and a combination of the two (mode I).[1] To prevent LMI, various strategies have been developed such as 3D electrode architectures;[2–5] electrolyte additives, *e.g.*, Cs salts;[6] and new SEI designs.[7] Recently, high concentrations of electrolyte salts, particularly the fluorinated ones, have been demonstrated capable of improving both (1) and (2) in LMA.[8,9] To avoid LMI, a common-sense approach might be to mitigate the parasitic reactions between the electrolytes and LMA. This favours the usage of cathodically more stable electrolytes, such as ionic liquids.[10–13]

Herein, we report that ethyl methyl sulfone (EMS) as a co-solvent in the ether-based electrolyte eliminates macroscopically observable LMI. Sulfone-containing electrolytes, including EMS, are known for their remarkable anodic stability but high cathodic reactivity.[14–17] Recently, high concentrations of salts solvated using sulfolane (TMS) have been studied on LMA as promising electrolytes.[18,19] In this work, we reveal that LMA exhibits dendrite-free plating/stripping behaviour in an electrolyte of 1 M bis(trifluoromethanesulfonyl)imide (LiTFSI) solvated in 50 v% of EMS, 25 v% 1,3-dioxolane (DOL), and 25 v% 1,2-dimethoxyethane (DME) (referred to as EMS/DOL/DME). However, in the Li||Cu asymmetric cells, LMA demonstrates a CE of only 30% in the above electrolyte. Surprisingly, elimination of macroscopic LMI does not necessarily lead to high CE.

We first employed Li||Li symmetric coin cells to reveal the impact of adding EMS as a co-solvent to the electrolyte. Scanning electron microscopy (SEM) imaging shows the surface morphology of LMA after 100 galvanostatic plating/stripping cycles at 1.0 mA cm^{-2} with a capacity of 1.0 mA h cm^{-2} in two electrolytes of 1 M LiTFSI in DOL/DME (50 v%/50 v%) (referred to as DOL/DME) and EMS/DOL/DME. In DOL/DME, LMA reveals a completely pulverized surface covered with lithium particles (Fig. 1a). In contrast, the EMS/DOL/DME electrolyte leads to an exceptionally flat and smooth surface entirely free of any LMI from the surface (Fig. 1b and c). This smooth configuration can be observed across the entire lithium metal surface, as shown in multiple-scale ranges (Fig. S1, ESI†). Similarly, the side view of LMA reveals the formation of mode-III LMI (Fig. 1d) in DOL/DME compared to no LMI formation in EMS/DOL/DME (Fig. 1e) by optical observation. The corresponding energy dispersive X-ray spectroscopy (EDX) elemental mappings reveal that the LMA's surface in the EMS/DOL/DME electrolyte is uniformly covered with sulphur- and fluorine-containing species, which constitute the SEI (Fig. S2, ESI†).

In situ optical microscopy imaging was performed in vial cells to monitor the morphological changes during the plating process at a current density of 0.3 mA cm^{-2} for 4 hours with a capacity of 1.2 mA h cm^{-2} in two different electrolytes (Fig. S3, ESI†). Fig. 1e shows that mossy-like LMI are formed during plating in the DOL/DME electrolyte (red arrows), and these are not fully removed during the following stripping process

[a] *Department of Chemistry, Oregon State University, Corvallis, OR, 97331, USA. E-mail: david.ji@oregonstate.edu*
[b] *Department of Nuclear Science and Engineering and Department of Materials Science and Engineering, Massachusetts Institute of Technology, Cambridge, MA, 02139, USA. E-mail: liju@mit.edu*
[c] *Hewlett-Packard Co., 1000 NE Circle Blvd., Corvallis, OR, 97330, USA*
[d] *Chemical Sciences and Engineering Division, Argonne National Laboratory, Argonne, IL, 60439, USA*

† Electronic supplementary information (ESI) available: Experimental details, EDX, *in situ* microscopy, and F_{1s} XPS. See DOI: 10.1039/c9cc00046a

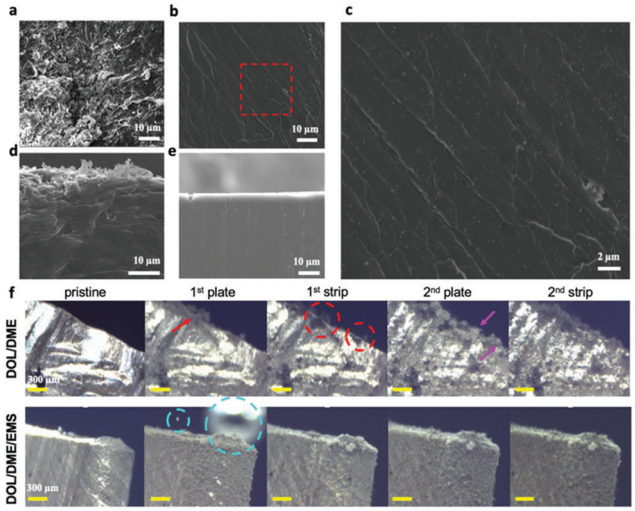

Fig. 1 Morphology studies on the cycled lithium surface. (a–e) SEM images of LMA examined after 100 cycles at 1.0 mA cm^{-2} with a capacity of 1.0 mA h cm^{-2}. LMA surface in (a) DOL/DME, (b) EMS/DOL/DME, and (c) an enlarged image of the red box shown in (b). Cross section images in (d) DOL/DME and (e) EMS/DOL/DME. (f) *In situ* optical images of LMA in DOL/DME (top) and EMS/DOL/DME (bottom) electrolytes. Current density is 0.3 mA cm^{-2} with a capacity of 1.2 mA h cm^{-2}. Arrows and circles in DOL/DME indicate LMI on LMA. Circles in the second image (bright blue) for EMS/DOL/DME denote the gas bubbles. The scale bar for all images is 300 μm.

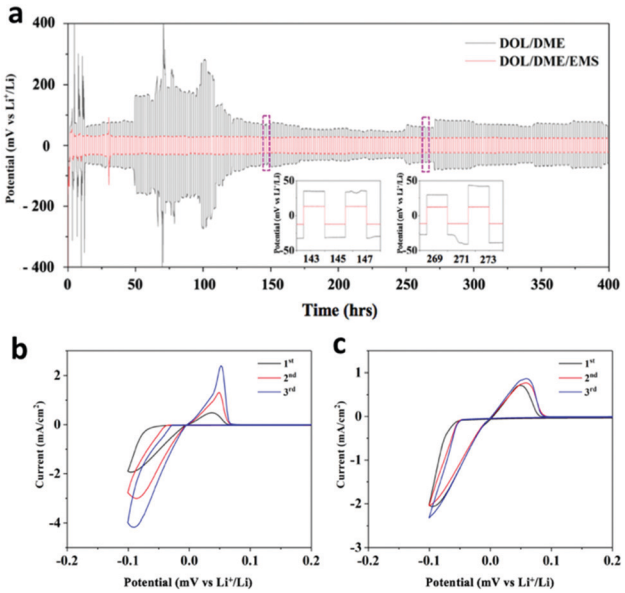

Fig. 2 (a) Electrochemical studies in Li||Li symmetric cells. Potential profiles of Li symmetric cells with the DOL/DME electrolyte and the EMS/DOL/DME electrolyte at a current density of 2.0 mA cm^{-2} with a capacity of 3.0 mA h cm^{-2}. Insets represent the 48th cycle (left) and the 90th cycle (right), respectively. CV profiles of the first three cycles in (b) DOL/DME and (c) EMS/DOL/DME.

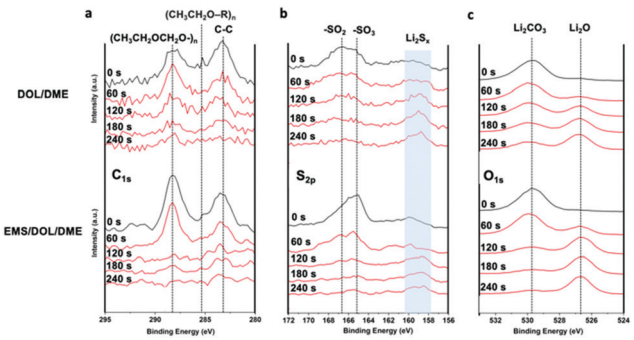

Fig. 3 The XPS profiles of the cycled LMA in the DOL/DME electrolyte (top) and the EMS/DOL/DME electrolyte (bottom) for (a) C_{1s}, (b) S_{2p} and (c) O_{1s}. Sputtering was carried out for 4 minutes with one scanning in every minute.

(red circles).[20] During the 2nd plating, LMI are formed on fresh lithium spots, where we expect that continuous 'dead' lithium formation will eventually cover the lithium upon cycling, consequently leading to lower CE. On the other hand, the EMS/DOL/DME electrolyte shows no obvious LMI formation and maintains the original surface morphology of LMA. However, during the first plating, bubbles are formed, which were not observed in DOL/DME. The bubble formation may release some of the carbon-containing moieties of EMS, thus leaving an SEI on the surface of LMA containing less organic but more inorganic constituents.

The galvanostatic plating/stripping tests using Li||Li symmetric cells at 2 mA cm^{-2} with a capacity of 3 mA h cm^{-2} reveal the performance juxtaposition of the two electrolytes. The DOL/DME electrolyte exhibits high overpotentials: from 50 to 110 cycles ranging from 150 to 400 mV and just below 100 mV afterwards (Fig. 2a and the inset), whereas the EMS/DOL/DME electrolyte exhibits consistently low overpotential of 15 mV.

Cyclic voltammetry (CV) tests of Li||Cu asymmetric cells where a Cu current collector serves as the working electrode reveal very different behaviours of LMA in electrolytes with or without EMS. In DOL/DME, the cathodic current and anodic current progressively increase during the initial three cycles (Fig. 3b), which indicates that LMA possesses a surface area anew and larger, after each cycle. However, in the EMS/DOL/DME electrolyte, the redox current remains stable during cycling, suggesting the markedly more stable surface of LMA, probably due to the favourable SEI formation (Fig. 3c). However, in the galvanostatic plating/stripping tests, the LMA exhibits a surprisingly low first-cycle CE of 30% (Fig. S4, ESI†), which indicates that the overwhelming majority of the plated lithium is consumed, *i.e.*, for building the SEI layer, which stems from the fact that EMS's reactivity toward lithium is very high.

Recently, the SEI layers on LMA are described by a dual-layer model with an organic layer on top of an inorganic layer. To understand the SEI structures of LMA in EMS/DOL/DME, we collected the *ex situ* XPS spectra of the LMA surface after 100 stripping/plating cycles with depth-profiling by Ar^+ sputtering. The entire sputtering process lasts for four minutes, where one spectrum was collected after every minute of sputtering. The results reveal that the LMA in EMS/DOL/DME comprises a thinner organic layer than the LMA in DOL/DME. The characteristic species of the organic layer of SEI, including Li_2CO_3, $(CH_3CH_2OCH_2O–)_n$,

$(CH_3CH_2O–R)_n$, and C–C peaks all disappear after two minutes of sputtering on LMA from EMS/DOL/DME, whereas all these peaks still remain on the LMA from DOL/DME even after sputtering for four minutes (Fig. 3a). A thinner organic layer of SEI on LMA in EMS/DOL/DME suggests that an inorganic layer of SEI formed with the assistance of EMS blocks the diffusion of DOL/DME solvent molecules.

We further studied the composition of the inorganic layer of SEI by sulphur and oxygen depth profiles (Fig. 3b and c). For both electrolytes, the $–SO_2$/$–SO_3$ peaks diminish along the depth, and both Li_2S_x ($1 \leq x \leq 2$) and Li_2O peaks emerge and grow upon further sputtering. Furthermore, the EMS/DOL/DME electrolyte shows a more rapid attenuation of the peaks for $–SO_2$/$–SO_3$ when going deeper during profiling. Compared to DOL/DME, EMS/DOL/DME exhibits weaker peak intensity of Li_2S and a more prominent presence of Li_2O. In addition, it is evident that EMS is preferentially decomposed over LiTFSI due to the fact that the fluorine signal only comes from the $TFSI^-$ anion, and the LMA in EMS/DOL/DME displays a weaker F_{1s} peak throughout the depth of SEI than in DOL/DME (Fig. S5, ESI†).

In summary, our results demonstrate that EMS completely suppresses macroscopic LMI on LMA, and facilitates extremely smooth surface morphology of LMA. The profiling XPS results reveal that EMS preferentially decomposes over DOL/DME and LiTFSI on the surface of LMA, generating a thinner organic layer near the electrode. Although EMS/DOL/DME does not seem to be practically apt as an electrolyte for LMA, its function to cause complete dendrite-free lithium plating warrants future attention on EMS as an electrolyte additive. We tentatively posit that the reaction between EMS and LMA may dramatically increase the total concentration of ions (ionic strength) near LMA, which prevents the formation of a Sand's extinction zone in the liquid where the ionic strength approaches zero.[21,22]

Conflicts of interest

There are no conflicts to declare.

Notes and references

1 S. Li, M. Jiang, Y. Xie, H. Xu, J. Jia and J. Li, *Adv. Mater.*, 2018, **30**, 1706375.
2 Z. Liang, D. Lin, J. Zhao, Z. Lu, Y. Liu, C. Liu, Y. Lu, H. Wang, K. Yan, X. Tao and Y. Cui, *PNAS*, 2016, **113**, 2862–2867.
3 Y. Zhang, W. Luo, C. Wang, Y. Li, C. Chen, J. Song, J. Dai, E. M. Hitz, S. Xu, C. Yang, Y. Wang and L. Hu, *PNAS*, 2017, **114**, 3584–3589.
4 G. Zheng, S. W. Lee, Z. Liang, H.-W. Lee, K. Yan, H. Yao, H. Wang, W. Li, S. Chu and Y. Cui, *Nat. Nanotechnol.*, 2014, **9**, 618–623.
5 X. Ji, D.-Y. Liu, D. G. Prendiville, Y. Zhang, X. Liu and G. D. Stucky, *Nano Today*, 2012, **7**, 10–20.
6 F. Ding, W. Xu, G. L. Graff, J. Zhang, M. L. Sushko, X. Chen, Y. Shao, M. H. Engelhard, Z. Nie, J. Xiao, X. Liu, P. V. Sushko, J. Liu and J.-G. Zhang, *J. Am. Chem. Soc.*, 2013, **135**, 4450–4456.
7 X.-B. Cheng, C. Yan, X. Chen, C. Guan, J.-Q. Huang, H.-J. Peng, R. Zhang, S.-T. Yang and Q. Zhang, *Chem*, 2017, **2**, 258–270.
8 L. Suo, W. Xue, M. Gobet, S. G. Greenbaum, C. Wang, Y. Chen, W. Yang, Y. Li and J. Li, *PNAS*, 2018, 201712895.
9 H.-G. Jung, J. Hassoun, J.-B. Park, Y.-K. Sun and B. Scrosati, *Nat. Chem.*, 2012, **4**, 579–585.
10 D. Aurbach, A. Zaban, A. Schechter, Y. Ein-Eli, E. Zinigrad and B. Markovsky, *J. Electrochem. Soc.*, 1995, **142**, 2873–2882.
11 C. Zu, N. Azimi, Z. Zhang and A. Manthiram, *J. Mater. Chem. A*, 2015, **3**, 14864–14870.
12 A. I. Bhatt, A. S. Best, J. Huang and A. F. Hollenkamp, *J. Electrochem. Soc.*, 2010, **157**, A66–A74.
13 G. H. Lane, P. M. Bayley, B. R. Clare, A. S. Best, D. R. MacFarlane, M. Forsyth and A. F. Hollenkamp, *J. Phys. Chem. C*, 2010, **114**, 21775–21785.
14 A. Abouimrane, I. Belharouak and K. Amine, *Electrochem. Commun.*, 2009, **11**, 1073–1076.
15 K. Xu and C. A. Angell, *J. Electrochem. Soc.*, 2002, **149**, A920–A926.
16 N. Shao, X.-G. Sun, S. Dai and D. Jiang, *J. Phys. Chem. B*, 2011, **115**, 12120–12125.
17 United States, US6245465B1, 2001.
18 J. Alvarado, M. A. Schroeder, M. Zhang, O. Borodin, E. Gobrogge, M. Olguin, M. S. Ding, M. Gobet, S. Greenbaum, Y. S. Meng and K. Xu, *Mater. Today*, 2018, **21**, 341–353.
19 X. Ren, S. Chen, H. Lee, D. Mei, M. H. Engelhard, S. D. Burton, W. Zhao, J. Zheng, Q. Li, M. S. Ding, M. Schroeder, J. Alvarado, K. Xu, Y. S. Meng, J. Liu, J.-G. Zhang and W. Xu, *Chem*, 2018, **4**, 1877–1892.
20 A. Kushima, K. P. So, C. Su, P. Bai, N. Kuriyama, T. Maebashi, Y. Fujiwara, M. Z. Bazant and J. Li, *Nano Energy*, 2017, **32**, 271–279.
21 M. D. Tikekar, S. Choudhury, Z. Tu and L. A. Archer, *Nat. Energy*, 2016, **1**, 16114.
22 H. J. S. Sand, *The London, Edinburgh, and Dublin Philosophical Magazine and Journal of Science*, 1901, **1**, 45–79.

Supporting Information

Ethyl Methyl Sulfone Co-Solvent Eliminates Macroscopic Morphological Instabilities of Lithium Metal Anode

Woochul Shin,[a] Kang Pyo So,[b] William F. Stickle,[c] Cong Su,[b] Jun Lu,[d] Ju Li,[b] Xiulei Ji[a]**

[a] Department of Chemistry, Oregon State University, Corvallis, OR, 97331, United States
[b] Department of Nuclear Science and Engineering and Department of Materials Science and Engineering, Massachusetts Institute of Technology, Cambridge, MA, 02139, United States
[c] Hewlett-Packard Co., 1000 NE Circle Blvd., Corvallis, OR, 97330, United States
[d] Chemical Sciences and Engineering Division, Argonne National Laboratory, Argonne, IL, 60439, United States

Corresponding Author

*Correspondence and requests for materials should be addressed to david.ji@oregonstate.edu; liju@mit.edu

Experimental Section

Li || Li and Li || Cu cell fabrication

Li metal ribbon was purchased from Aldrich (0.38mm thickness, 99.9% trace metal basis) and cut into 1cm diameter disk. Cu-foil was purchased from Advent-rm and immersed in 1 M HCl solution for 10 minutes followed by washing it with DI water and isopropyl alcohol three times respectively. 2032-type coin cells were fabricated in the glove box (MBRAUN Labmaster) under Ar atmosphere that has less than 1ppm of O_2 and H_2O. EMS was purchased from TCI America and purified by soaking lithium metal for two days. It was mixed with DOL/DME (BASF Corporation) in 1:1 volume ratio with 1 M LiTFSI (99%) that was purchased from Aldrich.

Characterization

Li || Li and Li || Cu cells were cycled using the Maccor cell tester at the room temperature for overpotential measurement and Coulombic efficiency test, respectively. Cycled Li metal was harvested by disassembling coin cells for SEM and XPS analysis in the glove box. For cyclic voltammetry test, BioLogics potentiostat was used in the scan rate of 1 mV/s. Cu foil was used as working electrode and lithium foil as working/reference electrode. SEM images of the Li electrodes were obtained with Quanta 600 FEG SEM with accelerating voltage of 5 kV. XPS data was obtained by PHI Quantera Scanning ESCA. The spectrometer uses a monochromatic aluminum X-ray source with a photon energy of 1486.6eV. The energy scale of the spectrometer is calibrated with Au 4f at 84.0 eV and Cu $2p^{3/2}$ at 932.7 eV. EIS impedance was measured by frequency change from 100 KHz to 10 mHz with potential amplitude of 10 mV. Sealed beaker cells are built for *in situ* optical microscopy study. Cu wire tethered lithium is connected to potentiostat for lithium deposition/stripping.

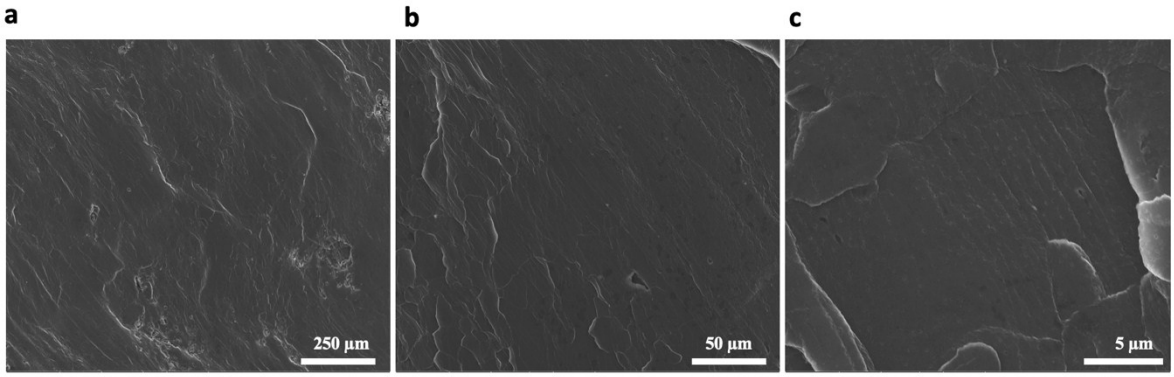

Fig. S1. Scanning electron microscopy (SEM) images of cycled lithium in DOL/DME/EMS electrolytes after 100 cycles at 1.0 mA cm^{-2} with a capacity of 1.0 mAh cm^{-2}. All three images show that EMS as a co-solvent can effectively suppress macroscopic morphological instabilities.

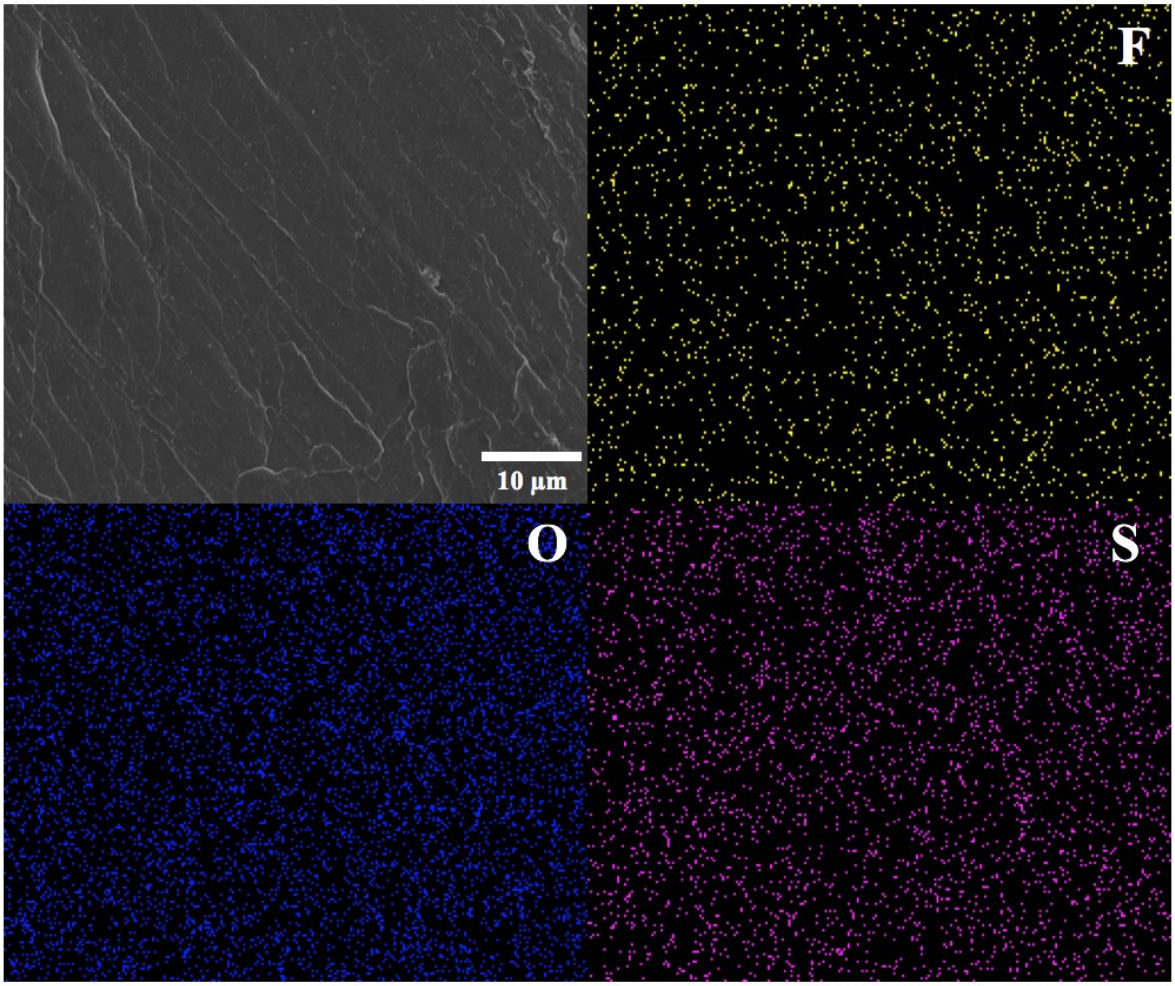

Fig. S2. EDX elemental mappings of the lithium surface: Fluorine, oxygen and sulfur. Before measurements, the LMA ran for 100 cycles at 1.0 mA cm^{-2} with a capacity of 1.0 mAh cm^{-2} in DOL/DME/EMS electrolyte.

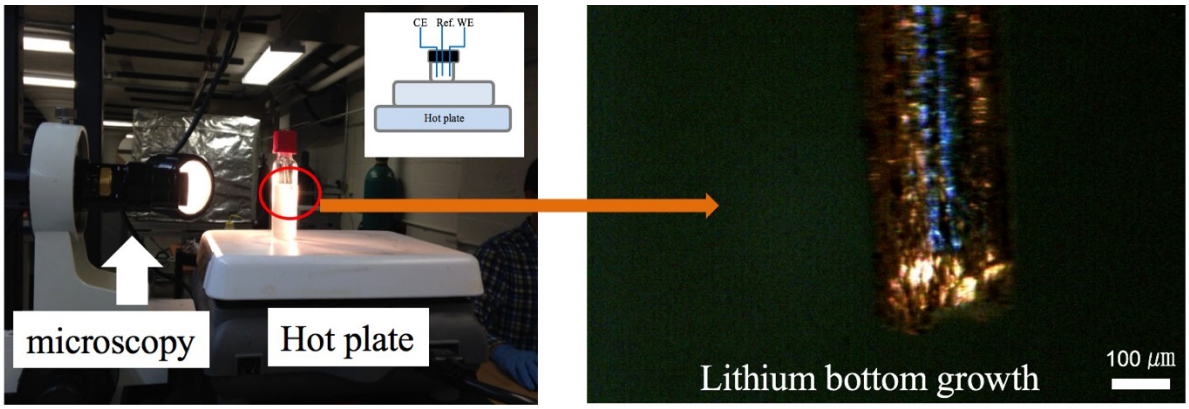

Fig. S3. *In situ* optical microscopy setup (left panel). Inset image shows the schematic design of three electrode vial cell. Right panel represents zoomed image of lithium rod inside a vial cell. The whole setup of the optical microscopy is placed on the air table to minimize the vibration and draft for a long period during Li deposition/stripping.

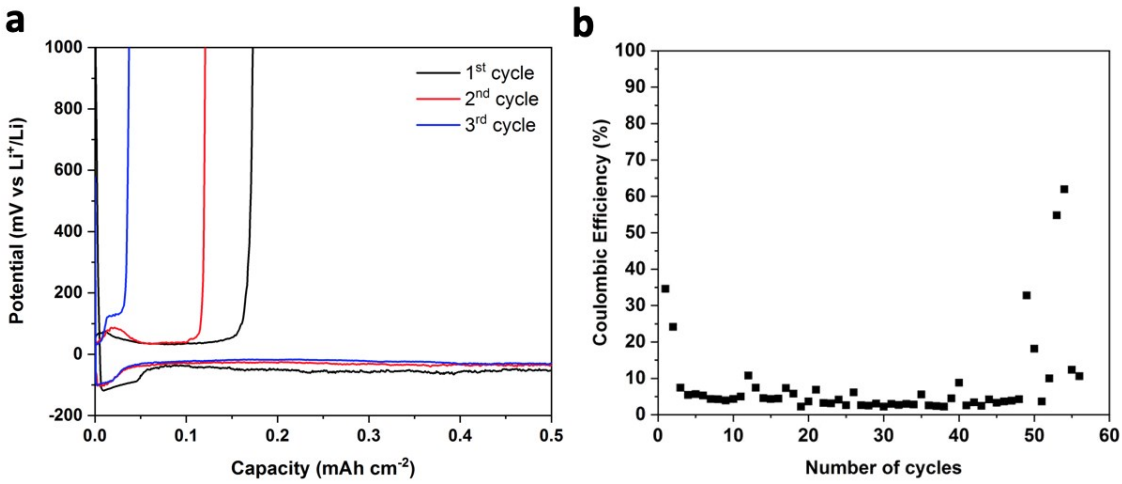

Fig. S4. The CE test in Li || Cu cells in the EMS/DOL/DME electrolyte. (a) GCD profiles of the first three cycles. (b) Plating/stripping CE over 60 cycles at 0.5 mA cm^{-2}. For each cycle, 0.5 mAh cm^{-2} of lithium is plated.

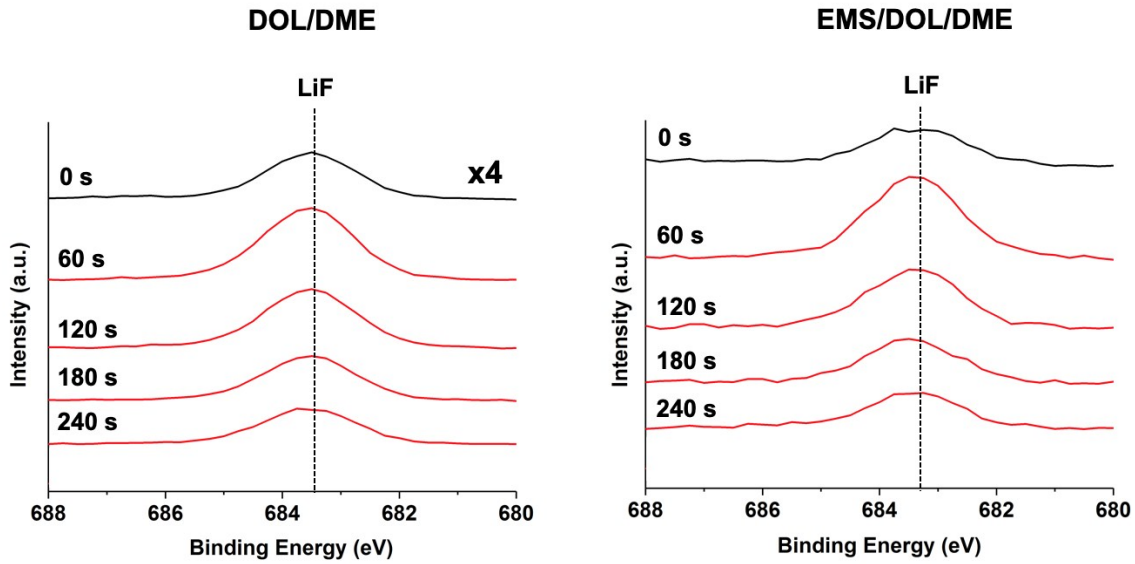

Fig. S5. The XPS F_{1s} profiles of the cycled LMA in DOL/DME electrolyte (left) and EMS/DOL/DME electrolyte (right). Note that LiF intensity of DOL/DME shows four times stronger than EMS/DOL/DME, supporting that $TFSI^-$ anion decomposition is suppressed by the preferential decomposition of EMS.